790 (1968).
[24]E. Daniel and S. H. Vosko, Phys. Rev. 120, 2041 (1960).
[25]D. J. W. Geldart, A. Houghton, and S. H. Vosko, Can. J. Phys. 42, 1938 (1964).

PHYSICAL REVIEW B VOLUME 3, NUMBER 6 15 MARCH 1971

Interband Absorption and the Optical Properties of Polyvalent Metals*

N. W. Ashcroft and K. Sturm
Laboratory of Atomic and Solid State Physics, Cornell University, Ithaca, New York 14850
(Received 21 May 1970)

Excitation of electrons between parallel or near-parallel one-electron bands in simple polyvalent metals constitutes a major source of the observed optical absorption. Much of the effect can be accounted for in a straightforward calculation of both real and imaginary parts of the conductivity, which does not require the constant-matrix-element assumption. In many cases, the magnitude and rounding of the absorption edges (singular in the absence of scattering) are quite sensitive to the phenomenological relaxation times (and hence to temperature) and to surface scattering. The sum rule for the (transverse) optical conductivity is related to the Fourier components of the weak periodic potential, and an expression is derived for the optical mass. The theory has been applied to study the optical properties of Al.

I. INTRODUCTION

Structure in the observed optical absorption from metals is normally related to singular behavior in the joint density of states associated with the single-particle bands. In polyvalent metals it is often found that by plotting the bands along certain directions in $\vec{k}$ space, a pair of them may be substantially parallel. This is the situation, for example, in Al,[1-4] and Ehrenreich *et al.*[5] observed that absorption edges of notable strength would go hand in hand with a parallel-band spectrum. The behavior of the absorption and the nature of the edge was partially analyzed for photon energies in the neighborhood of the threshold by Harrison,[6] who predicted (on the basis of independently calculated pseudopotentials) the position of absorption edges for a number of metals.

For energies sufficiently close to the edge, the oscillator strength required in Ref. 6 can be taken as effectively constant. In a more recent numerical calculation, Dresselhaus *et al.*[7] incorporated (among other things) the explicit $\vec{k}$ dependence of the oscillator strengths and obtained reasonable agreement with new data on Al reported in the same paper. Again, these data display prominent edges which reflect the presence of parallel bands (as noted in Ref. 6).

It is the purpose of this paper to demonstrate that the dominant features in the absorption actually follow quite straightforwardly from a simple weak-potential (or pseudopotential) representation of the important bands. We treat two cases: The first, in which scattering is assumed absent, is outlined in Sec. II and essentially reproduces for parallel-band absorption the results of Golovashkin *et al.*[8] We extend the analysis and derive an expression for the absorption which may be of interest at higher energies. To account for the broadening of the single-particle bands, we use a relaxation-time approximation result for the frequency-dependent conductivity (Sec. III). It is easy to show that the height of the edge is sensitive in this model to the choice of relaxation time τ, an observation which may account in some measure for the reported variations in the experimental values for $\sigma(\omega)$. For metals possessing one or more *small* band gaps ($\sim$few $\hbar/\tau$), it is apparent from the analysis that the broadening may extend to low energies, thereby adding to what is normally considered to be Drude, or intraband, scattering. The theory that follows is illustrated by explicitly evaluating both the real and imaginary parts of the optical conductivity $\sigma(\omega)$ for the cubic metal Al. (Generalization to noncubic systems is straightforward.) Determination of the surface and volume plasma frequency for Al from the imaginary part of the conductivity reveals good agreement with the results from electron energy-loss experiments. Finally, the contribution of the interband absorption to the sum rule for $\mathrm{Re}\sigma(\omega)$ is shown to lead to a simple relation involving the Fourier components (U_K) of the weak single-particle potential. It is also possible to derive an explicit relation for the optical effective mass in terms of the U_K's, whose compatibility with the requirements of the sum rule on the total (intraband and interband) absorption is easily demonstrated.

II. WEAK-POTENTIAL APPROXIMATION

The following analysis is restricted to metals whose bands are largely parabolic and only weakly perturbed by a small effective crystalline pseudopotential V. We assume that after the core states have been projected out from the problem the single-particle valence bands are described in a local pseudopotential approximation. They are given by the solution to the secular equation,

$$\det\{H_{\vec{K}\vec{K}'} - \delta_{\vec{K}\vec{K}'}\epsilon\} = 0 \quad , \tag{1}$$

where

$$\begin{aligned} H_{\vec{K}\vec{K}'} &= \delta_{\vec{K}\vec{K}'}\,\epsilon_{\vec{k}+\vec{K}} + V_{\vec{K}-\vec{K}'} \quad , \\ \epsilon_{\vec{k}+\vec{K}} &= (\hbar^2/2m)\,(\vec{k}+\vec{K})^2 \quad , \end{aligned} \tag{2}$$

and by choice $V_0 = 0$.

Provided there are no other nearby bands, the eigenvalues of (1) are given *near zone planes* by the solutions of

$$\begin{vmatrix} \epsilon_{\vec{k}} - \epsilon & U_{\vec{K}} \\ U_{\vec{K}} & \epsilon_{\vec{k}-\vec{K}} - \epsilon \end{vmatrix} = 0 \quad , \tag{3}$$

where, for the reciprocal-lattice vector $\vec{K}$ corresponding to the zone plane, we associate a "folded" Fourier component which is given to second order by

$$U_{\vec{K}} = V_{\vec{K}} + \sum_{\vec{K}' \neq \vec{K}} \frac{V_{\vec{K}'}\, V_{\vec{K}-\vec{K}'}}{\epsilon_{\vec{k}} - \epsilon_{\vec{k}-\vec{K}'}} \quad .$$

It is the quantity $U_{\vec{K}}$ which is usually given in the analysis of Fermi-surface data, assuming (as is frequently the case) that any $\vec{k}$ dependence is weak. Corresponding to the reduced secular equation (3) we may take wave functions

$$\psi_{\vec{k}} = \Omega^{-1/2}\,(c_{\vec{k}}\, e^{i\vec{k}\cdot\vec{r}} + c_{\vec{k}-\vec{K}}\, e^{i(\vec{k}-\vec{K})\cdot\vec{r}}) \quad , \tag{4}$$

where for correct normalization in a volume Ω the coefficients are readily shown to be given by[9]

$$c^2_{\vec{k}} = \tfrac{1}{2}\left(1 + \frac{\gamma}{(1+\gamma^2)^{1/2}}\right), \qquad c^2_{\vec{k}-\vec{K}} = \tfrac{1}{2}\left(1 - \frac{\gamma}{(1+\gamma^2)^{1/2}}\right) \quad , \tag{5}$$

with

$$\gamma = \frac{\hbar^2}{2m}\,\frac{(\vec{k}-\vec{K})^2 - \vec{k}^2}{2U_K} = \frac{\hbar^2}{2m}\,\frac{K^2 - 2k_{\parallel}K}{2U_K} = \frac{\epsilon_{\vec{K}}\,(1 - 2k_{\parallel}/K)}{2U_K}$$

(where we have resolved $\vec{k}$ into its components parallel and transverse to $\vec{K}$; viz., $\vec{k} = \vec{k}_{\parallel} + \vec{k}_{\perp}$). In the same notation the energy of the upper (+) and lower (−) bands is found from (3) to be

$$\epsilon = (\hbar^2/2m)\,\{k_{\perp}^2 + k_{\parallel}^2\} + |\,U_{\vec{K}}\,|\,[\,|\gamma| \pm (1+\gamma^2)^{1/2}] \quad . \tag{6}$$

These are plotted[10] in the extended-zone scheme in Fig. 1 and clearly show the parallel nature of the bands when mapped in either the (111) or (200) faces, or planes parallel to them (i.e., fixed $k_{\parallel}$, see Fig. 2).

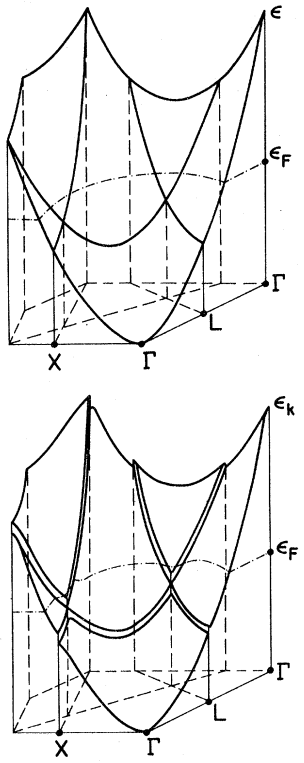

FIG. 1. (a) Empty lattice free-electron bands in Al appropriate to a section in a (110) plane; (b) splitting of degenerate bands and appearance of parallel bands due to a small effective crystal potential.

When scattering is absent, the contribution to the conductivity $\sigma(\omega)$ from interband absorption is given to second order by

$$\sigma_{IB}(\omega) = \frac{e^2}{a_0\hbar}\,\frac{\pi\hbar^3 a_0}{3\Omega m^2\omega}\sum_{n'n\vec{k}} f(\epsilon_{n\vec{k}})\,|\langle\psi_{n'\vec{k}}\,|\,\vec{\nabla}\,|\,\psi_{n\vec{k}}\rangle\,|^2 \times \delta(\epsilon_{n'\vec{k}} - \epsilon_{n\vec{k}} - \hbar\omega) \quad , \tag{7}$$

with the restriction that the final states $(n'\vec{k})$ are empty.[11] In the case of polyvalent metals, we consider the absorption in two parts. First, there is absorption between lower and upper bands as shown in Fig. 2. All optical interband transitions are between states of constant interband energy difference and are thus restricted to parallel bands. By plotting the bands in the zone face, as in Fig. 2, this parallelism is clearly displayed. We will follow Harrison and refer to this allowed first-zone–second-zone absorption as "parallel band" absorption. Second, there is the familiar interband absorption considered by Butcher and others[12] [see Fig. 3(a)] which (although also parallel in the sense described above) we will refer to as normal interband absorption. In either case we proceed to evaluate (7) by converting the sum over $\vec{k}$ into the usual integral and taking for the element $d\vec{k}$

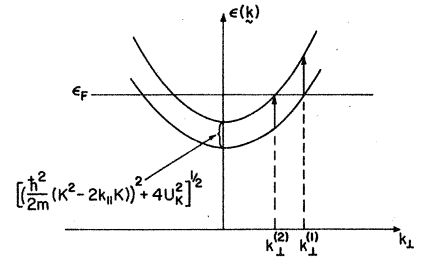

FIG. 2. Form of the energy bands mapped in a plane parallel to the (111) or (200) face. Vertical arrows indicate parallel-band absorption.

$$d\vec{k} = 2\pi k_\perp dk_\perp dk_\parallel \quad . \tag{8}$$

Further, using (4) and (5) we find after a little manipulation

$$\langle \psi_{2\vec{k}} \,|\, \vec{\nabla} \,|\, \psi_{1\vec{k}} \rangle = \tfrac{1}{2} i \vec{K} (1+\gamma^2)^{-1/2} \quad ,$$

where we have taken $n=2$ for the upper band and $n=1$ for the lower. Then (7) becomes

$$\sigma_{IB}(\omega) = \sigma_a \frac{\epsilon_K}{\omega} \left(\frac{a_0\hbar}{m}\right) \int dk_\parallel (2k_\perp dk_\perp) \frac{f(\epsilon_{1\vec{k}})}{1+\gamma^2} \times \delta[2|U_K|(1+\gamma^2)^{1/2} - \hbar\omega] \quad , \tag{9}$$

where $\epsilon_K = (\hbar^2/2m)K^2$, and[13] $\sigma_a = (e^2/a_0\hbar)(24\pi)^{-1}$.

For the case of parallel-band absorption σ_{PB} we write (9) as

$$\sigma_{PB}(\omega) = \sigma_a \frac{\epsilon_K}{\omega} \frac{a_0\hbar}{m} \int dk_\parallel [k_\perp^2]_1^2 \frac{f(\epsilon_{1k})}{1+\gamma^2} \times \delta[2|U_K|(1+\gamma^2)^{1/2} - \hbar\omega] \quad ,$$

where

$$[k_\perp^2]_1^2 = \{k_\perp^{(2)}\}^2 - \{k_\perp^{(1)}\}^2 \quad ,$$

and where, for fixed $k_\parallel$ and Fermi energy ϵ_F, we find from (6)

$$[k_\perp^2]_1^2 = K^2 (2|U_K|/\epsilon_K)(1+\gamma^2)^{1/2} \, .$$

Hence we have

$$\sigma_{PB}(\omega) = \sigma_a (a_0 K) \frac{2\epsilon_K}{\hbar\omega} \int \frac{dk_\parallel}{K} \frac{2|U_K|(1+\gamma^2)^{1/2}}{1+\gamma^2} \times f(\epsilon_{1\vec{k}}) \delta[2|U_K|(1+\gamma^2)^{1/2} - \hbar\omega] \quad ,$$

and after making a simple change in variable $x = 2|U_K|(1+\gamma^2)^{1/2}$ the integration is elementary, giving

$$\sigma_{PB}(\omega) = \sigma_a (a_0 K)(2U_K/\hbar\omega)^2/[1-(2U_K/\hbar\omega)^2]^{1/2} \, . \tag{10}$$

Equation (10) gives the absorption between parallel bands in the neighborhood of a single-zone plane. This result has previously been obtained by Golovashkin *et al.*[8] and is discussed in the recent review article by Motulevich.[14]

Parallel-band absorption [as given by (10)] terminates for frequencies ω_0, where, neglecting terms second order in (U_K/ϵ_F) [see Eq. (A3)],

$$\hbar\omega_0 = \epsilon_K[(2k_F/K) - 1]$$

Note that (10) predicts an edge at $\hbar\omega_e$ when $\hbar\omega_e = |2U_K|$. For frequencies slightly in excess of ω_e we have

$$\sigma_{PB}(\omega) = \sigma_a (|2U_K|)^{3/2}/[\hbar\omega(\hbar\omega - |2U_K|)^{1/2}] \quad , \tag{11}$$

a form similar to that derived by Harrison.[6] It is also worth pointing out explicitly that, away from the edge, the absorption goes as ω^{-2}, a dependence similar to that found in the Drude term. As an example of the behavior of (10), we plot in Fig. 4 $\sigma_{PB}(\omega)$ for the (111) and (200) sets of planes in Al, taking as values for U_{111} and U_{200} the pseudopotential components that reproduce the measured Fermi surface (Ref. 4).

We turn now to the normal (or Butcher-type) interband absorption $\sigma_N(\omega)$. From (9) we have

$$\sigma_N(\omega) = \sigma_a \frac{\epsilon_K}{\omega} \frac{a_0\hbar}{m} \int dk_\parallel [k_\perp^2] \frac{f(\epsilon_{1k})}{1+\gamma^2} \times \delta[2|U_K|(1+\gamma^2)^{1/2} - \hbar\omega] \, ,$$

where now we have for $k_\perp^2$ (at a given $k_\parallel$)

$$k_\perp^2(k_\parallel) = K^2 g(k_\parallel) \quad ,$$

with

$$g(k_\parallel) = \frac{\epsilon_F}{\epsilon_K} - \left(\frac{k_\parallel}{K}\right)^2 - \frac{|U_K|}{\epsilon_K}[|\gamma| - (1+\gamma^2)^{1/2}] \quad .$$

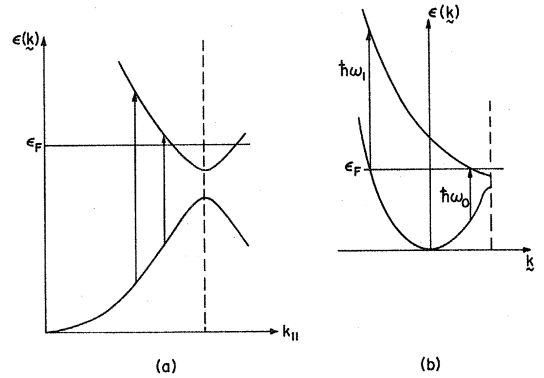

FIG. 3. (a) Normal-interband absorption; (b) $\hbar\omega_0$ and $\hbar\omega_1$ define the points in the frequency spectrum where normal interband absorption begins and ends, respectively.

Then

$$\sigma_N(\omega) = \sigma_a \frac{\epsilon_K^2 2a_0}{\hbar\omega} \int dk_\parallel\, g(k_\parallel)\, \frac{1}{1+\gamma^2} \times \delta\left[2\left|U_K\right|(1+\gamma^2)^{1/2} - \hbar\omega\right]$$

$$= \sigma_a \frac{(a_0 K)\,\epsilon_K}{\hbar\omega} \left|2U_K\right|^2 \times \int dx\, \frac{g(x)}{[1-(2U_K/x)^2]^{1/2}} \frac{1}{x^2}\, \delta(x-\hbar\omega)$$

$$= \sigma_a (a_0 K) \frac{\epsilon_K}{\hbar\omega} \left(\frac{2U_K}{\hbar\omega}\right)^2 \frac{g(\hbar\omega)}{[1-(2U_K/\hbar\omega)^2]^{1/2}} . \tag{12}$$

We show in the Appendix that

$$g(\hbar\omega) = (4\epsilon_K^2)^{-1} (\hbar\omega + \hbar\omega_0)(\hbar\omega_1 - \hbar\omega) \quad ,$$

where ω_1 marks the frequency at which absorption terminates in the two-band model [Fig. 3(b)]. Then (12) becomes

$$\sigma_N(\omega) = \sigma_a (a_0 K) \frac{(2U_K/\hbar\omega)^2}{[1-(2U_K/\hbar\omega)^2]^{1/2}} \times \frac{(\hbar\omega + \hbar\omega_0)(\hbar\omega_1 - \hbar\omega)}{4\hbar\omega\,\epsilon_K} \quad , \tag{13}$$

which, apart from the factor $[1-(2U_K/\hbar\omega)^2]^{-1/2}$ is similar in form to Butcher's result. Contributions from (13) join continuously onto the parallel-band absorption given by (10) as shown schematically in Fig. 5. Equations (10) and (13) give the contributions expected from absorption in the neighborhood

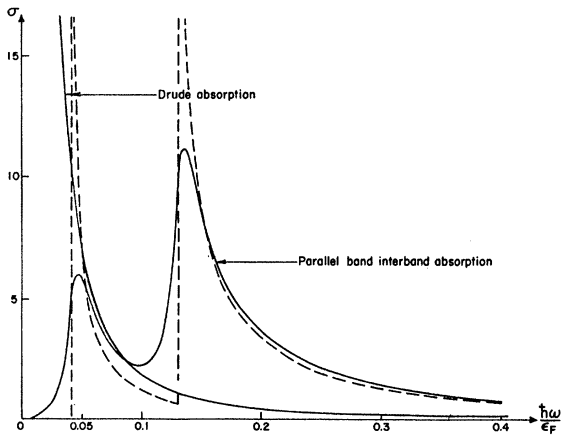

FIG. 4. Dashed curves show the parallel-band absorption in Al in the absence of scattering [Eq. (10)]. Solid curves give the individual contributions to the absorption, namely, the Drude and parallel-band absorption. For both the same scattering rate was assumed; $\tau = 0.6\times10^{-14}$ sec. σ is always measured in units of $\sigma_a 2a_0 k_F = 1.014\times10^{15}$ sec^{-1}.

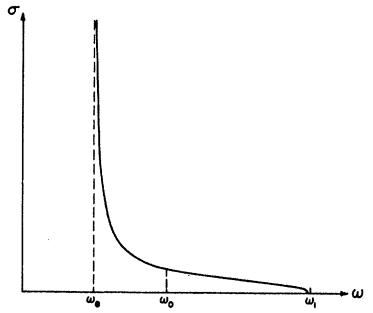

FIG. 5. Combined parallel-band and normal-interband absorption (collisionless case).

of a single-zone plane. To obtain the total absorption corresponding to the entire first zone we simply weight these results by the appropriate number of planes[15] bounding the zone. This procedure will necessarily overlook some additional fine structure in the absorption arising at points of higher symmetry (at W and K, for example, in Al). These have considerably smaller phase-space and oscillator strengths.

III. COLLISION EFFECTS

Effects of interband scattering processes can be included by introducing a semiphenomenological relaxation time τ and replacing (7) by[16]

$$\sigma_{IB}(\omega) = \frac{e^2/a_0\hbar}{i\omega} \frac{\pi a_0 \hbar}{3m^2\Omega} \times \sum_{\vec{k}} \left(\frac{\hbar\omega}{\epsilon_{2\vec{k}} - \epsilon_{1\vec{k}}}\right)^2 \left|\langle\psi_{2\vec{k}}\left|\vec{\nabla}\right|\psi_{1\vec{k}}\rangle\right|^2 f(\epsilon_{1\vec{k}}) \times \left(\frac{1}{\epsilon_{2\vec{k}} - \epsilon_{1\vec{k}} - \hbar(\omega + i/\tau)} + \frac{1}{\epsilon_{2\vec{k}} - \epsilon_{1\vec{k}} + \hbar(\omega + i/\tau)}\right) . \tag{14}$$

Equation (14) is the two-band case of the more familiar expression

$$\sigma_{IB}(\omega) = \frac{e^2/a_0\hbar}{i} \frac{\pi a_0 \hbar^3}{3m\Omega}\, \omega \sum_{\vec{k}\, n'n} F_{n'n}(\vec{k}) \times \left[(\epsilon_{n'\vec{k}} - \epsilon_{n\vec{k}})^2 - \hbar\left(\omega + \frac{i}{\tau}\right)^2\right]^{-1} , \tag{15}$$

where

$$F_{n'n}(\vec{k}) = \frac{2}{(\epsilon_{n'\vec{k}} - \epsilon_{n\vec{k}})m} \left|\langle\psi_{n'\vec{k}}\left|\vec{\nabla}\right|\psi_{n\vec{k}}\rangle\right|^2$$

is the oscillator strength and satisfies the f sum rule

$$\sum_{n'} F_{n'n}(\vec{k}) = 1 - \frac{m}{3\hbar^2} \nabla_{\vec{k}}^2\, \epsilon_n(\vec{k}) . \tag{16}$$

Note that (14) reduces to (7) in the limit $1/\tau \to 0$, and with (15) is written in a form that suggests

[through (16)] particle conservation during the collision process.[17] Now we may write (14) as

$$\sigma_{IB}(\omega) = \frac{\sigma_a(a_0K)}{i\hbar\omega}\,\frac{\epsilon_K^2}{\pi|U_K|}\int\frac{dk_\parallel}{K} \times\left[\frac{k_\perp^2(k_\parallel)}{K^2}\right]\left(\frac{\hbar\omega}{2U_K(1+\gamma^2)^{1/2}}\right)^2\frac{1}{1+\gamma^2} \times\left(\frac{1}{(1+\gamma^2)^{1/2}-z-ib}+\frac{1}{(1+\gamma^2)^{1/2}+z+ib}\right), \quad (17)$$

where we have put

$$z=\hbar\omega/2|U_K|, \quad b=\hbar/(2\tau|U_K|), \text{ and } b/z=1/\omega\tau.$$

Introducing $y=1+\gamma^2$ we find for the real part of the parallel-band contribution to σ

$$\mathrm{Re}\sigma_{PB}(\omega)=\sigma_a(a_0K)|\hbar\omega/2U_K|/\pi \times\int_1^{z_0^2}\frac{dy}{(y-1)^{1/2}}\,\frac{1}{y}\,\frac{2zb}{y^2+2(b^2-z^2)y+(z^2+b^2)^2}. \quad (18)$$

The integral here is straightforward to evaluate, and we may write the result as [cf. Eq. (10)]

$$\mathrm{Re}\sigma_{PB}(\omega)=\sigma_a(a_0K)\left|\frac{2U_K}{\hbar\omega}\right|^2\left\{\left[1-\left(\frac{2U_K}{\hbar\omega}\right)^2-\left(\frac{1}{\omega\tau}\right)^2\right]^2+\frac{4}{(\omega\tau)^2}\right\}^{-1/4}\frac{(\omega\tau)^2}{1+(\omega\tau)^2}\,J(\omega). \quad (19)$$

The function $J(\omega)$ tends quickly to unity for $(\hbar\omega)^2>(2U_K)^2+(\hbar/\tau)^2$ [and over all, $\sigma(\omega)\sim\omega$ for small ω]. $J(\omega)$ is defined by

$$J(\omega)=\frac{4zb\rho}{\pi(z^2+b^2)}\tan^{-1}t_0+\frac{1}{2\pi}\left(\frac{z^2-b^2}{z^2+b^2}\cos\phi+\frac{2zb}{z^2+b^2}\sin\phi\right)\ln\left(\frac{t_0^2+2t_0\rho\sin\phi+\rho^2}{t_0^2-2t_0\rho\sin\phi+\rho^2}\right) +\frac{1}{\pi}\left(\frac{z^2-b^2}{z^2+b^2}\sin\phi-\frac{2zb}{z^2+b^2}\cos\phi\right)\left[\tan^{-1}\left(\frac{t_0+\rho\sin\phi}{\rho\cos\phi}\right)+\tan^{-1}\left(\frac{t_0-\rho\sin\phi}{\rho\cos\phi}\right)\right],$$

where

$$\phi=\tfrac{1}{2}\left[\tfrac{5}{3}\pi-\tan^{-1}\left(\frac{1+b^2-z^2}{2bz}\right)\right],$$

$$\rho^2=[(1+b^2-z^2)^2+4z^2b^2]^{1/2},$$

$$z_0=\hbar\omega_0/2|U_K|, \quad t_0=(z_0^2-1)^{1/2}.$$

When we have $(\hbar\omega)^2>(2U_K)^2+(\hbar/\tau)^2$, (19) gives, to high accuracy, the collisionless result (10). For reasonable values of τ the effect of collisions on the *normal* interband absorption can be neglected entirely, although they are straightforward to include.[18]

By way of illustration, we compare in Figs. 6 the numerical results of Dresselhaus *et al.*[7] for $\mathrm{Re}\sigma(\omega)$ in Al with the predictions of (19). The value of τ which seems to fit the principal (room-temperature) interband absorption is $\tau=0.5\times10^{-14}$ sec. Note that part of the scattering rate $1/\tau$ may be due to surface scattering, a component that will be present even at low temperatures. To include this we use the results of Holstein and Dingle,[19] namely, that if the electrons scatter *diffusely* at the surface the effective scattering rate is given by

$$1/\tau_s=\tfrac{3}{8}(v_F/c)(4\pi ne^2/m)^{1/2}.$$

In the simplest approximation, we assume additivity of bulk and surface scattering rates

$$1/\tau=1/\tau_s+1/\tau_{\mathrm{bulk}}. \quad (20)$$

(There is also some question about the correct value of the bulk scattering rate. As Holstein and Gurzhi[20] pointed out, in the optical and infrared frequency regime for temperatures T smaller than the Debye temperature θ, τ_{bulk} is not simply the relaxation time derived from the dc conductivity but is modified by quantum effects. Gurzhi gives an explicit formula which relates the effective τ_{bulk} to the dc relaxation time τ_{dc},

$$1/\tau_{\mathrm{bulk}}=\varphi(T)(1/\tau_{\mathrm{dc}}),$$

where in the present situation $\varphi(T)$ is given by

$$\varphi(T)\approx\tfrac{2}{5}\left(\frac{\theta}{T}\right)+4\left(\frac{T}{\theta}\right)^4\int_0^{\theta/T}dv\,\frac{v^4}{e^v-1}.$$

With $\theta=390\,^\circ$K for Al, this leads to a slight enhancement of the bulk scattering rate by $\varphi(T)=1.075$; with $\tau_{\mathrm{dc}}=0.75\times10^{-14}$ sec, Eq. (20) yields a value for τ very near to 0.5×10^{-14}.) In Fig. 6(a) we compare the experimental result derived by a Kramers-Kronig analysis from reflectivity data by Beaglehole[7] with the theoretical result calculated with (19) and $\tau=0.5\times10^{-14}$. At liquid-nitrogen temperature (77 °K), the enhancement factor becomes $\varphi(T)=\frac{2}{5}\theta/T=2$. But this strong enhancement of the bulk scattering rate is not particularly effective

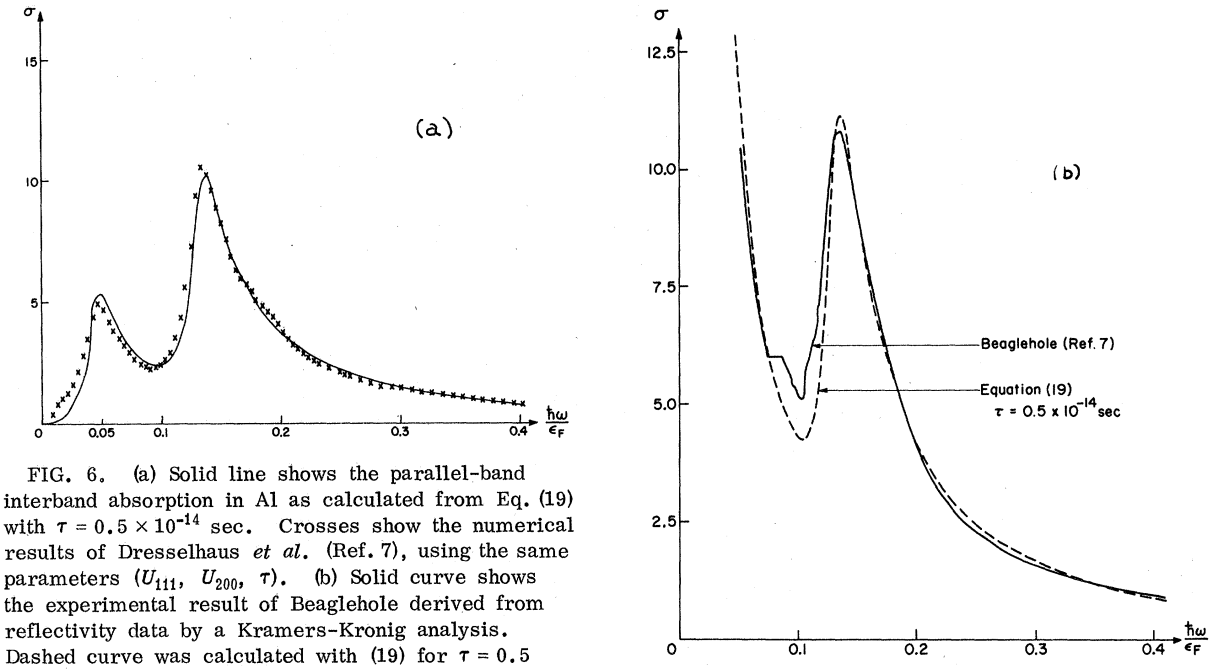

FIG. 6. (a) Solid line shows the parallel-band interband absorption in Al as calculated from Eq. (19) with $\tau = 0.5 \times 10^{-14}$ sec. Crosses show the numerical results of Dresselhaus *et al.* (Ref. 7), using the same parameters (U_{111}, U_{200}, τ). (b) Solid curve shows the experimental result of Beaglehole derived from reflectivity data by a Kramers-Kronig analysis. Dashed curve was calculated with (19) for $\tau = 0.5 \times 10^{-14}$ sec.

since at this temperature surface scattering dominates. In Fig. 7 we compare the theoretical absorption curve at liquid-nitrogen temperature ($T = 77\,^\circ$K, $\tau = 1.135 \times 10^{-14}$ sec) with the corresponding curve for room temperature ($T = 300\,^\circ$K, $\tau = 0.5 \times 10^{-14}$ sec). It is quite apparent that the structure arising from the interband absorption due to the (111) gap is almost entirely concealed by the Drude absorption.[21] In this energy range and at very low temperatures, only faint structure has been observed.[22]

IV. INTERBAND CONTRIBUTION TO Imσ (ω) AND DETERMINATION OF SURFACE AND VOLUME PLASMA FREQUENCY

We now turn to the imaginary part of the conductivity, which is related to the polarizability $\alpha(\omega)$ by

$$\alpha(\omega) = (1/\omega)\mathrm{Im}\sigma(\omega) \ .$$

Including collisions from the outset we find from (14) and (17) (in the same notation) the parallel-band contributions to $\mathrm{Im}\sigma(\omega)$ to be

$$\mathrm{Im}\sigma_{\mathrm{PB}} = \sigma_a(a_0k)\,\frac{z}{\pi}\,\mathrm{Re}\int_1^{z_0} \frac{dx}{x^2(x^2-1)^{1/2}} \times \left(\frac{1}{x-z-ib} + \frac{1}{x+z+ib}\right) . \tag{21}$$

The integral is again quite straightforward to evaluate and the result is also in terms of simple functions. It is, however, more complex than (19). We find

$$\mathrm{Im}\sigma_{\mathrm{PB}} = \sigma_a(a_0k)\,\frac{1}{2b\pi\rho}\left(\frac{1}{2}\sin\phi_1 \ln\left(\frac{z_0^2-1+2(z_0^2-1)^{1/2}\rho\cos\phi_1+\rho^2}{z_0^2-1-2(z_0^2-1)^{1/2}\rho\cos\phi_1+\rho^2}\right)\right.$$

$$+\cos\phi_1\left[\tan^{-1}\left(\frac{(z_0^2-1)^{1/2}+\rho\cos\phi_1}{\rho\sin\phi_1}\right)+\tan^{-1}\left(\frac{(z_0^2-1)^{1/2}-\rho\cos\phi_1}{\rho\sin\phi_1}\right)\right]$$

$$+\frac{b^2-z^2}{b^2+z^2}\left\{\frac{4bz\rho}{b^2+z^2}\tan^{-1}(z_0^2-1)^{1/2}+\frac{1}{2}\left(\frac{z^2-b^2}{z^2+b^2}\cos\phi_2+\frac{2zb}{z^2+b^2}\sin\phi_2\right)\right.$$

$$\left.\left.\times\ln\left(\frac{z_0^2-1+2(z_0^2-1)^{1/2}\rho\sin\phi_2+\rho^2}{z_0^2-1-2(z_0^2-1)^{1/2}\rho\sin\phi_2+\rho^2}\right)\right\}\right)$$

$$+\frac{z^2-b^2}{z^2+b^2}\left(\sin\phi_2-\frac{2zb}{z^2+b^2}\cos\phi_2\right)\left[\tan^{-1}\left(\frac{(z_0^2-1)^{1/2}+\rho\sin\phi_2}{\rho\cos\phi_2}\right)+\tan^{-1}\left(\frac{(z_0^2-1)^{1/2}-\rho\sin\phi_2}{\rho\cos\phi_2}\right)\right]\Bigg\}\Bigg), \tag{22}$$

where

$$\phi_1=\frac{1}{2}\left[\frac{1}{2}\pi+\tan^{-1}\left(\frac{1+b^2-z^2}{2zb}\right)\right], \quad \phi_2=\frac{1}{2}\left[\frac{1}{2}\pi-\tan^{-1}\left(\frac{1+b^2-z^2}{2zb}\right)\right],$$

$$\rho=[(1+b^2-z^2)^2+4z^2b^2]^{1/4}.$$

The essential features are more easily observed from the limiting case $1/\pi\to 0$ (i.e., $b\to 0$). For $\hbar\omega<\hbar\omega_e$ ($\hbar\omega_e=2|U_K|$) we obtain

$$\mathrm{Im}\sigma_{\mathrm{PB}}=\sigma_a(a_0K)\frac{4}{\pi}\frac{|U_K|}{\hbar\omega}\times\left[\frac{1}{[1-(\hbar\omega/2U_K)^2]^{1/2}}\tan^{-1}\left(\frac{(\hbar\omega_0/2U_K)^2-1}{[1-(\hbar\omega/2U_K)^2]^{1/2}}\right)\tan^{-1}[(\hbar\omega_0/2U_K)^2-1]^{1/2}\right], \tag{23}$$

whereas for $\hbar\omega>\hbar\omega_e=2|U_K|$ we obtain

$$\mathrm{Im}\sigma_{\mathrm{PB}}=\sigma_a(a_0K)\frac{4}{\pi}\frac{|U_K|}{\hbar\omega}\times\left(\frac{1}{2[(\hbar\omega/2U_K)^2-1]^{1/2}}\ln\left|\frac{[(\hbar\omega_0/2U_K)^2-1]^{1/2}-[(\hbar\omega/2U_K)^2-1]^{1/2}}{[(\hbar\omega_0/2U_K)^2-1]^{1/2}+[(\hbar\omega/2U_K)^2-1]^{1/2}}\right|-\tan^{-1}[(\hbar\omega_0/2U_K)^2-1]^{1/2}\right). \tag{24}$$

The form of this result is displayed in Fig. 8 together with the curve derived with the inclusion of collisions. The effect of collisions proves again to be quite pronounced ($\tau=0.5\times10^{-14}$ sec). In Fig. 9 we compare our result with the experimental curve of Dusselhaus *et al.*[7] obtained by Kramers-Kronig analysis from the re-

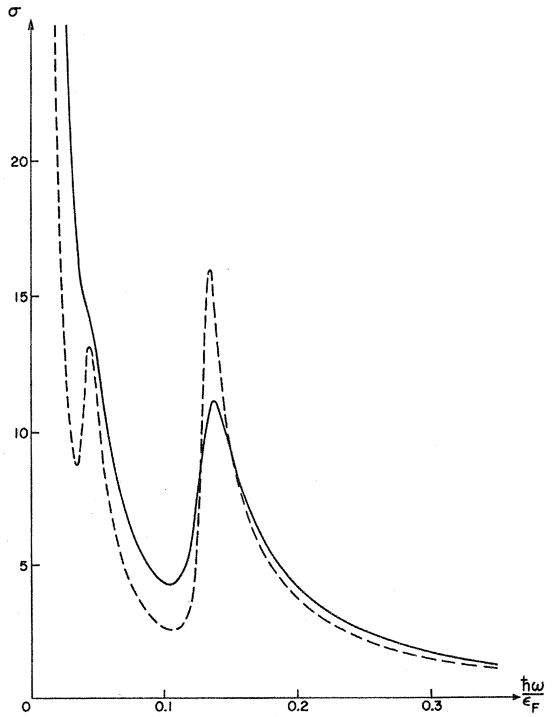

FIG. 7. Dashed curve shows the predicted total absorption in Al at liquid-nitrogen temperature. Solid curve shows the total absorption at room temperatures where $\tau=0.5\times10^{-14}$ sec was assumed to fit the experimental data (Ref. 7).

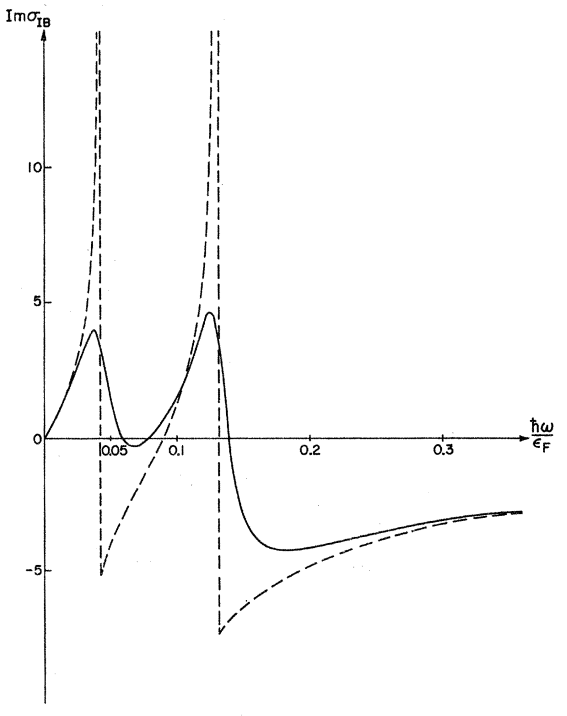

FIG. 8. Dashed curves display the parallel-band contribution to $\mathrm{Im}\sigma(\omega)$. Solid curve shows the effect of collisions on $\mathrm{Im}\sigma_{\mathrm{PB}}(\omega)$.

flectivity. The crosses represent numerical results obtained by Dresselhaus *et al.*,[7] using the same parameters.

Starting from (14) the contributions to $\mathrm{Im}\sigma(\omega)$ from "normal" bands are easily found to be

$$\mathrm{Im}\sigma_{\mathrm{IB}}^{N} = \sigma_a(a_0K)\,\frac{z}{\pi}\,\frac{|U_K|}{2\epsilon_K}\,\mathrm{Re}\int_{z_0}^{z_1}\frac{dx\,(x+z_0)(z_1-x)}{x^3(x^2-1)^{1/2}}\left(\frac{1}{x-z-ib}+\frac{1}{x+z+ib}\right)\quad . \tag{25}$$

Although the general result (i.e., including the effect of collisions) can easily be obtained in term of simple functions, we restrict ourselves here to the limit $1/\tau \to 0$ (i.e., $b \to 0$) and find for $\hbar\omega < \hbar\omega_e = 2|U_K|$

$$\begin{aligned}\mathrm{Im}\sigma_{\mathrm{IB}}^{N} &= \sigma_a(a_0K)\,\frac{1}{\pi}\,\frac{|U_K|}{\epsilon_K}\\
&\times\Bigg\{\frac{\hbar\omega_0\hbar\omega_1-(\hbar\omega)^2}{(\hbar\omega)^2[1-(\hbar\omega/2U_K)^2]^{1/2}}\left[\tan^{-1}\left(\frac{\hbar\omega}{\hbar\omega_1}\,\frac{[(\hbar\omega_1/2U_K)^2-1]^{1/2}}{[1-(\hbar\omega/2U_K)^2]^{1/2}}\right)-\tan^{-1}\left(\frac{\hbar\omega}{\hbar\omega_0}\,\frac{[(\hbar\omega_0/2U_K)^2-1]^{1/2}}{[1-(\hbar\omega/2U_K)^2]^{1/2}}\right)\right]\\
&-\frac{\hbar\omega_0}{\hbar\omega}\,[(\hbar\omega_1/2U_K)^2-1]^{1/2}+\frac{\hbar\omega_1}{\hbar\omega}\,[(\hbar\omega_0/2U_K)^2-1]^{1/2}\\
&+\frac{\hbar\omega_1-\hbar\omega_0}{\hbar\omega[1-(\hbar\omega/2U_K)^2]^{1/2}}\left[\tan^{-1}\left(\frac{[(\hbar\omega_1/2U_K)^2-1]^{1/2}}{[1-(\hbar\omega/2U_K)^2]^{1/2}}\right)-\tan^{-1}\left(\frac{[(\hbar\omega_0/2U_K)^2-1]^{1/2}}{[1-(\hbar\omega/2U_K)^2]^{1/2}}\right)\right]\\
&-\frac{\hbar\omega_1-\hbar\omega_0}{\hbar\omega}\,\{\tan^{-1}[(\hbar\omega_1/2U_K)^2-1]^{1/2}-\tan^{-1}[(\hbar\omega_0/2U_K)^2-1]^{1/2}\}\Bigg\}.\end{aligned} \tag{26}$$

For $\hbar\omega > \hbar\omega_e$

$$\begin{aligned}\mathrm{Im}\sigma_{\mathrm{IB}}^{N} &= \sigma_a(a_0K)\,\frac{1}{\pi}\,\frac{|U_K|}{\epsilon_K}\\
&\times\Bigg(\frac{\hbar\omega_0\hbar\omega_1-(\hbar\omega)^2}{2(\hbar\omega)^2[(\hbar\omega/2U_K)^2-1]^{1/2}}\ln\left|\frac{\hbar\omega_1[(\hbar\omega/2U_K)^2-1]^{1/2}-\hbar\omega[(\hbar\omega_1/2U_K)^2-1]^{1/2}}{\hbar\omega_1[(\hbar\omega/2U_K)^2-1]^{1/2}+\hbar\omega[(\hbar\omega_1/2U_K)^2-1]^{1/2}}\right.\\
&\left.\times\frac{\hbar\omega_0[(\hbar\omega/2U_K)^2-1]^{1/2}+\hbar\omega[(\hbar\omega_0/2U_K)^2-1]^{1/2}}{\hbar\omega_0[(\hbar\omega/2U_K)^2-1]^{1/2}-\hbar\omega[(\hbar\omega_0/2U_K)^2-1]^{1/2}}\right|\\
&-\frac{\hbar\omega_0}{\hbar\omega}\,[(\hbar\omega_1/2U_K)^2-1]^{1/2}+\frac{\hbar\omega_1}{\hbar\omega}\,[(\hbar\omega_0/2U_K)^2-1]^{1/2}+\frac{\hbar\omega_1-\hbar\omega_0}{2\hbar\omega[(\hbar\omega/2U_K)^2-1]^{1/2}}\\
&\times\ln\left|\frac{[(\hbar\omega/2U_K)^2-1]^{1/2}-[(\hbar\omega_1/2U_K)^2-1]^{1/2}}{[(\hbar\omega/2U_K)^2-1]^{1/2}+[(\hbar\omega_1/2U_K)^2-1]^{1/2}}\,\frac{[(\hbar\omega/2U_K)^2-1]^{1/2}+[(\hbar\omega_0/2U_K)^2-1]^{1/2}}{[(\hbar\omega/\hbar U_K)^2-1]^{1/2}-[(\hbar\omega_0/2U_K)^2-1]^{1/2}}\right|\\
&-\frac{\hbar\omega_1-\hbar\omega_0}{\hbar\omega}\,\{\tan^{-1}[(\hbar\omega_1/2U_K)^2-1]^{1/2}-\tan^{-1}[(\hbar\omega_0/2U_K)^2-1]^{1/2}\}\Bigg)\quad .\end{aligned} \tag{27}$$

In the frequency regime considered here the contributions to $\mathrm{Im}\sigma(\omega)$ from normal bands are relatively small (see Fig. 10) and their addition to the parallel-band contribution causes very little change. Having now derived the dominant band-structure contributions to the polarizability, we are able to determine the plasma frequency. The well-known longitudinal plasma mode has a frequency satisfying $\mathrm{Re}\epsilon(\omega)=0$. $\mathrm{Re}\epsilon(\omega)$ is related to the polarizability or $\mathrm{Im}\sigma(\omega)$ by

$$\mathrm{Re}\epsilon(\omega) = 1 + 4\pi\alpha(\omega) = 1 + 4\pi\mathrm{Im}\sigma(\omega)/\omega\ .$$

We now assume that $\mathrm{Im}\sigma(\omega)$ contains the following contributions:

(i) the "free-electron" polarization (Drude part)[23,24]

$$4\pi\alpha_D = (4\pi ne^2/m_{\mathrm{opt}})/\omega^2\ ;$$

(ii) the parallel-band contribution [Eq. (24)]

$$4\pi\alpha_{\mathrm{PB}} = 4\pi\mathrm{Im}\sigma_{\mathrm{PB}}/\omega\ ;$$

(iii) and the normal-band contribution [Eq. (27)]

$$4\pi\alpha_{\mathrm{IB}}^{N}(\omega) = 4\pi\,\mathrm{Im}\sigma_{\mathrm{IB}}^{N}/\omega\ .$$

Hence the plasma frequency ω_P (which is measured, for example, in electron-energy-loss experiments)[25]

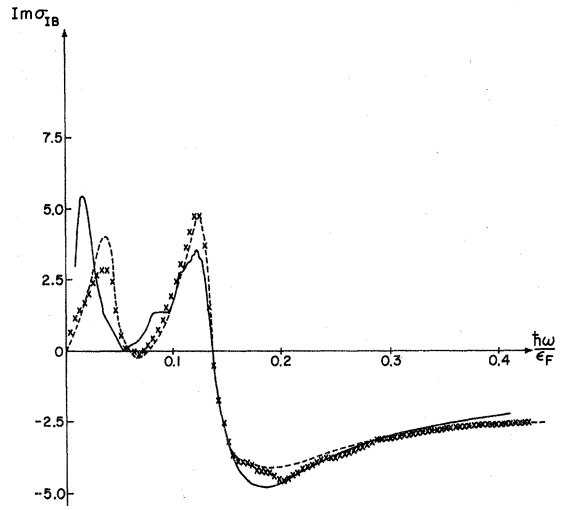

FIG. 9. Solid line shows experimental result of Dresselhaus *et al.* (Ref. 7) derived from reflectivity data by a Kramers-Kronig analysis. Dashed curve is calculated with Eq. (22) for $\tau = 0.5 \times 10^{-14}$ sec. Crosses represent the theoretical results of Dresselhaus *et al.* (Ref. 7), using the same values for U_{111}, U_{200}, and τ.

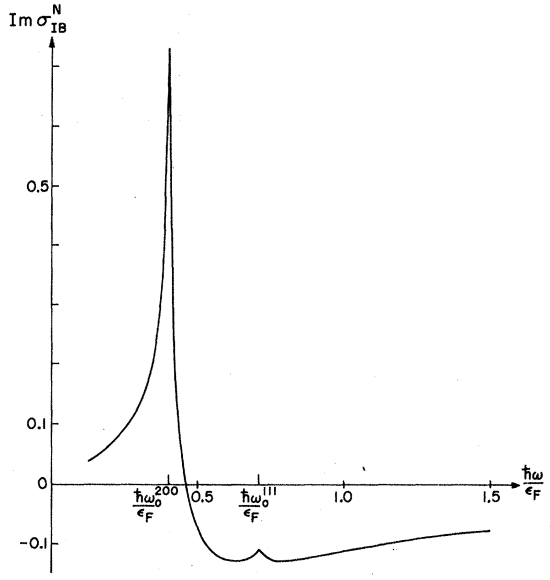

FIG. 10. $\mathrm{Im}\sigma^N_{IB}$, the normal-band contribution to the imaginary part of the conductivity for the limiting case $1/\tau \to 0$.

is determined from

$$4\pi\alpha_{tot}(\omega_p) = 4\pi(\alpha_D + \alpha_{PB} + \alpha^N_{IB}) = -1 \ . \tag{28}$$

From Fig. 11 we observe $\hbar\omega_p = 15.3$ eV for Al. Together with the (volume) plasmon $\hbar\omega_p$, energy-loss experiments also reveal a collective surface excitation, the surface plasmon, whose excitation energy $\hbar\omega_{sp}$ (for a vacuum metal interface) in the simplest approximation is determined by

$$\mathrm{Re}\epsilon(\omega_{sp}) = -1 \ ,$$

i.e.,

$$4\pi\alpha_{tot}(\omega_{sp}) = -2 \ . \tag{29}$$

Again from Fig. 11 we obtain $\hbar\omega_{sp} = 10.8$ eV for Al. These values agree very well with the experimental results by Powell and Swan[25] ($\hbar\omega_{sp} = 10.3$ eV and $\hbar\omega_p = 15.3$ eV) and provide a useful test of the internal consistency of the theory outlined above.

V. SUM RULES, OPTICAL MASS, AND DISCUSSION

We have pointed out that in the vicinity of points of high symmetry in the zone we expect additional interband absorption, an effect which is not included in the weighted two-band model. Since the bands quickly become nearly free-electron-like away from these points, the phase space for these processes is by no means as favorable as that available for parallel-band absorption. Examination of the typical magnitudes predicted by either Eq. (10) or Eq. (19) suggests strongly that the interband absorption in polyvalent metals should be dominated by σ_{PB}, and any other structure will give rise to only small corrections (as is apparently the case in Al).

The physical reason behind the strong parallel-band absorption can be seen in from Eq. (7). The energy-conserving δ function requires

$$\epsilon_{n'\vec{k}} - \epsilon_{n\vec{k}} = \hbar\omega \ ,$$

which clearly defines a surface of constant energy difference, say $S_{n'n}(\vec{k})$. Now

$$\sum_k f(\epsilon_{n\vec{k}}) |\langle\psi_{n'\vec{k}}| \vec{\nabla} |\psi_{n\vec{k}}\rangle|^2 \delta(\epsilon_{n'\vec{k}} - \epsilon_{n\vec{k}} - \hbar\omega)$$

$$= \frac{V}{4\pi^3} \int d\vec{k} f(\epsilon_{n\vec{k}}) |\langle\psi_{n'\vec{k}}| \vec{\nabla} |\psi_{n\vec{k}}\rangle|^2 \delta(\epsilon_{n'\vec{k}} - \epsilon_{n\vec{k}} - \hbar\omega) \ , \tag{30}$$

and instead of using (8) let us write

$$d\vec{k} = dS_{n'n}(\vec{k}) \frac{d(\epsilon_{n'\vec{k}} - \epsilon_{n\vec{k}} - \hbar\omega)}{|\nabla_{\vec{k}}(\epsilon_{n'\vec{k}} - \epsilon_{n\vec{k}} - \hbar\omega)|} \ .$$

It is now clear that if the matrix element $|\langle\psi_{n'\vec{k}}|\vec{\nabla}|\psi_{n\vec{k}}\rangle|$ were to be set constant, then (30) simply gives us a quantity proportional to the joint density of states. As it is, the matrix element is, in general, not constant but any singular behavior in $|\nabla_{\vec{k}}(\epsilon_{n'\vec{k}} - \epsilon_{n\vec{k}} - \hbar\omega)|$ will still persist. At a zone plane, the bands in the two-band model are both parallel and flat; $|\nabla_{\vec{k}}(\epsilon_{n'\vec{k}} - \epsilon_{n\vec{k}} - \hbar\omega)|$ vanishes and is not integrated out (as singular behavior with a smaller phase space frequently is). The result is an absorption edge and the scale of the parallel-

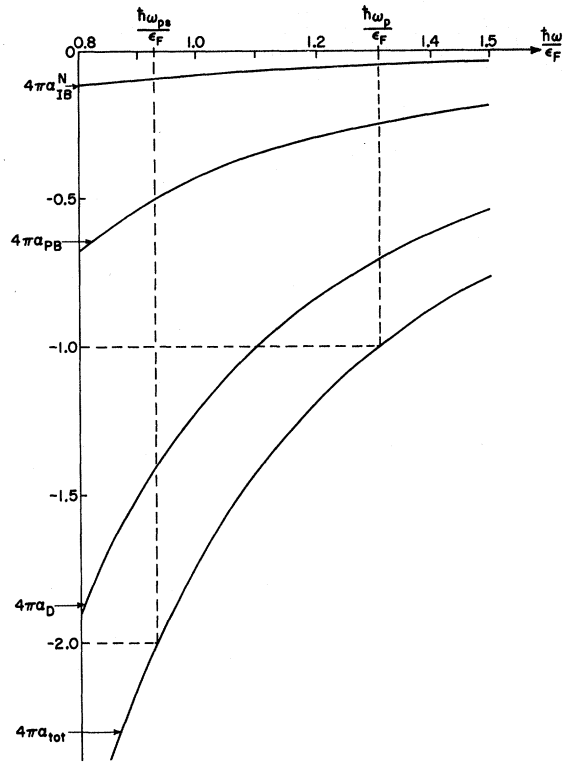

FIG. 11. Individual contributions to the polarizability $\alpha(\omega)$ and the total polarizability are plotted in the high-frequency regime and used to derive $\hbar\omega_{sp}$ and $\hbar\omega_p$ for Al.

band interband absorption is significantly larger than the normal interband absorption.[26]

Scattering processes broaden the interband absorption edge. These may be due to impurities, phonons, surface scattering, and even final-state interactions. Much of the scattering is temperature dependent and according to (19) the peaks in σ should rise with decreasing scattering rate (we find that, approximately, $\sigma_{max}\sim\tau$). Notice that when the band gap in the metal is small (say a few $\hbar/\tau$), the corresponding interband absorption may be significant enough to interfere with the familiar Drude absorption. The latter is[27]

$$\sigma_D(\omega)=\frac{ne^2\tau/m_{opt}}{1+(\omega\tau)^2}=\sigma_a(2a_0k_F)\,\frac{8}{\pi}\,\frac{\epsilon_F/(\hbar/\tau)}{1+(\omega\tau)^2}\,\frac{m}{m_{opt}} \tag{31}$$

or

$$\sigma_D(\omega)=\sigma_a(2a_0k_F)\,\frac{8}{\pi}\left(\frac{\epsilon_F}{\hbar\omega}\right)^2\frac{\hbar/\tau}{\epsilon_F}\,\frac{m}{m_{opt}} \tag{32}$$

for $\omega\tau>1$. The Drude contribution shown in Fig. 4 is plotted using (31). The optical mass m_{opt} can be obtained as follows: The usual definition for a cubic system is

$$\frac{m}{m_{opt}}=\frac{\hbar m}{12\pi^3 n}\int_{FS} dS v_{\vec{k}} \tag{33}$$

(where FS stands for surface integration over the Fermi surface), which may be rewritten

$$\frac{m}{m_{opt}}=\frac{m}{12\pi^3 n\hbar^2}\int d^3\vec{k}\nabla_k^2\epsilon_k\,, \tag{34}$$

where the integral is taken over the occupied states. Using Eq. (6) we find

$$\frac{1}{3}\nabla_k^2\epsilon_k=\frac{\hbar^2}{m}\pm\frac{1}{3}\frac{\epsilon_K}{|U_K|}\frac{\hbar^2}{2m}(1+\gamma^2)^{-3/2}\,,$$

where again (+) refers to the upper band and (−) to the lower. Using (6) again the contributions from the two bands taken together (after a little rearranging) give

$$1-\frac{m}{m_{opt}}=\frac{1}{4}\frac{K}{2k_F}\frac{|2U_K|}{\epsilon_F}\int_1^{z_0}\frac{dx}{x(x^2-1)^{1/2}}+\frac{1}{4}\frac{K}{2k_F}\times\frac{U_K^2}{\epsilon_K\epsilon_F}\int_{z_0}^{z_1}\frac{dx}{x^2(x^2-1)^{1/2}}(x+z_0)(z_1-x)\,. \tag{35}$$

Before we evaluate (35) explicitly, we turn to the sum rules. For the transverse conductivity we have[28]

$$\int_0^\infty d\omega\,\mathrm{Re}\sigma(\omega)=\tfrac{1}{2}\pi(ne^2/m)\,. \tag{36}$$

For the sake of simplicity we restrict ourselves to the collisionless situation for which

$$\int_0^\infty d\omega\left(\frac{1}{2}\delta(\omega)\frac{ne^2\pi}{m_{opt}}+\mathrm{Re}\sigma_{IB}(\omega)\right)=\frac{1}{2}\pi\frac{ne^2}{m}\,, \tag{37}$$

which we may write as

$$\frac{1}{4}\frac{1}{2a_0k_F}\frac{1}{\sigma_a}\int_0^\infty\frac{\hbar d\omega}{\epsilon_F}\sigma_{IB}(\omega)=1-\frac{m}{m_{opt}}\,. \tag{38}$$

From (10) the contribution for a single-zone plane to the left-hand side of (38) is shown to be

$$S_K^{(1)}=\frac{1}{4}\frac{K}{2k_F}\frac{2|U_K|}{\epsilon_F}\int_1^{z_0}\frac{dx}{x(x^2-1)^{1/2}}=\frac{1}{4}\frac{K}{2k_F}\frac{2|U_K|}{\epsilon_F}\left[\frac{\pi}{2}-\sin^{-1}\left(\frac{2|U_K|}{\hbar\omega_0}\right)\right], \tag{39}$$

and is the first term on the right-hand side of (35). This accounts for parallel-band absorption. For the remainder we find from (13)

$$S_K^{(2)}=\frac{1}{4}\frac{K}{2k_F}\frac{U_K^2}{\epsilon_K\epsilon_F}\int_{z_0}^{z_1}\frac{dx}{x^2(x^2-1)^{1/2}}(x+z_0)(z_1-x)\,, \tag{40}$$

which is the second term on the right-hand side of (35). We have demonstrated directly that the oscillator strength removed from the Drude term appears in the interband term, as required by the sum rule. Note that $S_K^{(1)}$ is essentially linear in U_K and dominates both the optical mass and the contribution to

TABLE I. Contribution of parallel-band $\sum S_K^{(1)}$ and normal-interband $\sum S_K^{(2)}$ optical absorption to sum rule [Eqs. (39) and (41)].

	$\sum S_K^1$	$\sum S_K^2$	Total
{111}	0.0975	0.0021	0.0996
{200}	0.2160	0.0370	0.2530

the sum rule, i.e.,

$$S_K^{(1)} = \frac{1}{8}\,\pi \frac{K}{2k_F}\left|\frac{2U_K}{\epsilon_F}\right| .$$

To second order we may write (40) as

$$S_K^{(2)} = \frac{1}{4}\,\frac{K}{2k_F}\,\frac{U_K^2}{\epsilon_K \epsilon_F}\left[\frac{\omega_0}{2\omega_1} + \frac{3\omega_1}{2\omega_0} - 2 - \ln\left(\frac{\omega_1}{\omega_0}\right)\right] . \quad (41)$$

Equations (39) and (41) have been applied to Al with the result shown in Table I. It is clear that to $O(U_K^2)$ the lower bands exhaust about one-third of the electrons contributing.

To the same order in the potential we find for the optical mass

$$1 - \frac{m}{m_{\rm opt}} = \sum_K \frac{1}{2}\,\frac{K}{2k_F}\,\frac{|U_K|}{\epsilon_F}\left\{\left[\frac{\pi}{2} - \sin^{-1}\left(\frac{2U}{\hbar\omega_0}\right)\right] + \frac{|U_K|}{2\epsilon_K} \times \left[\frac{\omega_0}{2\omega_1} + \frac{3\omega_1}{2\omega_0} - 2 - \ln\left(\frac{\omega_1}{\omega_0}\right)\right]\right\} , \quad (42)$$

which, for Al, gives $m_{\rm opt} = 1.55m$. (This value is in good agreement with Brust's recent computer calculations[29] of the optical properties of Al in which an optical mass $m_{\rm opt} = 1.45$ is found.) The Drude contribution shown in Fig. 4 is plotted using a value of $m_{\rm opt} = 1.55m$. Note that the relative contributions of Drude and interband absorption are given for $\hbar\omega > |2U_K|$ by combining (32) and (10),

$$\frac{\sigma_D(\omega)}{\sigma_{PB}(\omega)} = \frac{2}{\pi}\,\frac{2k_F}{K}\,\frac{\epsilon_F}{U_K}\,\frac{\hbar/\tau_0}{U_K}\,\frac{m}{m_{\rm opt}} . \quad (43)$$

This shows that although for a small band gap ϵ_F/U_K may be large, the resulting factor may be entirely nullified by $(\hbar/\tau)/U_K$. The overlapping of interband and Drude absorption may lead to difficulties in assigning optical effective masses if the former is assumed absent. [In addition many polyvalent metals possess lines of band contact[4] which happen to cut their Fermi surfaces, thereby permitting interband absorption (with ever decreasing phase space) down to the near static limit.]

The analysis given above is applicable to those metals with nearly free-electron-like bands. It is clear from (43), and (10) or (19), that in metals with substantial band gaps the parallel-band absorption is large and easily identifiable and should therefore be a useful guide to the approximate determination of the U_K.[30] Note that the excitation of the electrons to and from assumed single-particle states involves (in this problem) energy differences amounting to several eV. It follows that energy dependence of the pseudopotential may not be a negligible effect and should be included if the theory is extended. To use (19) as a basis for extracting information on the Fourier components of the potential, it is clearly advantageous to work in a regime where the Drude absorption is comparatively weak. Furthermore, by comparing (for a given metal) the variation of absorption peak heights with, say, impurity content, it should be possible to infer information on the energy dependence of the interband-scattering rate. Finally, many-body effects seem unlikely to be important at energies away from the edge (but less than the plasmon energy). Since scattering is exceedingly important *at* the edge,[31] it is at least conceivable that effects having their origin beyond the single-particle picture may be of some interest here.

ACKNOWLEDGMENT

We are very grateful to Dr. N. Smith for his critical comments on the manuscript and for acquainting us with some of the extensive literature on the subject of optical properties of metals.

APPENDIX

Let $\hbar\omega_0$ be the energy at which parallel-band absorption ceases and normal interband absorption commences. Let $\hbar\omega_1$ be the energy at which normal interband absorption ceases (see Fig. 3).

Now the value of $k_\parallel$ corresponding to the first case is given by the solution to

$$\begin{vmatrix} \frac{\hbar^2}{2m}(K - k_\parallel)^2 - \epsilon_F & U_K \\ U_K & \frac{\hbar^2}{2m}k_\parallel^2 - \epsilon_F \end{vmatrix} = 0, \quad (A1)$$

and of the second by $-\bar{k}_\parallel$, $(\bar{k}_\parallel > 0)$, where

$$\begin{vmatrix} \frac{\hbar^2}{2m}\bar{k}_\parallel^2 - \epsilon_F & U_K \\ U_K & \frac{\hbar^2}{2m}(K - \bar{k}_\parallel)^2 - \epsilon_F \end{vmatrix} = 0 . \quad (A2)$$

Since the energy-conserving δ function requires

$$k_\parallel = \tfrac{1}{2}K\left\{1 - \frac{\hbar\omega}{\epsilon_K}\left[1 - \left(\frac{2U_K}{\hbar\omega}\right)^2\right]^{1/2}\right\} ,$$

then the frequencies corresponding to $k_\parallel$ and $-\bar{k}_\parallel$ are given by the roots of [for either (A1) or (A2)]

$$\begin{vmatrix} \frac{\hbar^2}{2m}\left(\frac{K}{2}\right)^2\left\{1+\frac{\hbar\omega}{\epsilon_K}\left[1-\left(\frac{2U_K}{\hbar\omega}\right)^2\right]^{1/2}\right\}^2-\epsilon_F & U_K \\ U_K & \frac{\hbar^2}{2m}\left(\frac{K}{2}\right)^2\left\{1-\frac{\hbar\omega}{\epsilon_K}\left[1-\left(\frac{2U_K}{\hbar\omega}\right)^2\right]^{1/2}\right\}^2-\epsilon_F \end{vmatrix} = 0 .$$

The roots are

$$\hbar\omega_0 = 2(\epsilon_K\epsilon_F + U_K^2)^{1/2} - \epsilon_K , \qquad \text{(A3)}$$

$$\hbar\omega_1 = 2(\epsilon_K\epsilon_F + U_K^2)^{1/2} + \epsilon_K , \qquad \text{(A4)}$$

with the consequence that

$$\hbar\omega_1 - \hbar\omega_0 = 2\epsilon_K .$$

Now we have

$$g(\hbar\omega) = \frac{\epsilon_F}{\epsilon_K} - \left(\frac{k_\parallel}{K}\right)^2 - \frac{|U_K|}{\epsilon_k}\left[\,|\gamma| - (1+\gamma^2)^{1/2}\,\right],$$

where

$$\gamma = (\epsilon_K/2|U_K|)(1 - 2k_\parallel/K) ,$$

$$2|U_K|(1+\gamma^2)^{1/2} = \hbar\omega .$$

It follows that

$$k_\parallel/K = \tfrac{1}{2}[1 - (2U_K/\epsilon_K)\gamma] ,$$

and accordingly,

$$g(\hbar\omega) = \frac{\epsilon_F}{\epsilon_K} - \tfrac{1}{4}\left[1+\left(\frac{2U_K}{\epsilon_K}\right)^2\gamma^2\right] + \frac{|U_K|}{\epsilon_K}(1+\gamma^2)^{1/2}$$

$$= \frac{1}{4\epsilon_K^2}\left\{4\epsilon_K\epsilon_F - \epsilon_K^2 - (4U_K^2)\left[\left(\frac{\hbar\omega}{2U_K}\right)^2 - 1\right] + 2\hbar\omega\,\epsilon_K\right\}$$

$$= \frac{1}{4\epsilon_K^2}(\hbar\omega + \hbar\omega_0)(\hbar\omega_1 - \hbar\omega)$$

using (A3) and (A4).

*Work supported in part by the National Science Foundation (Grant No. GP-14802) and in part by the Advanced Research Projects Agency through the Materials Science Center at Cornell University, Ithaca, N. Y., MSC Report No. 1356.

[1]V. Heine, Proc. Roy. Soc. (London) A240, 340 (1957); A240, 354 (1957); A240, 361 (1957).

[2]W. A. Harrison, Phys. Rev. 118, 1182 (1960); 118, 1190 (1960).

[3]B. Segall, Phys. Rev. 124, 1797 (1960).

[4]N. W. Ashcroft, Phil. Mag. 8, 2055 (1963). By construction the bands here accurately fit the observed Fermi-surface structure.

[5]H. Ehrenreich, H. R. Phillip, and B. Segall, Phys. Rev. 132, 1918 (1963).

[6]W. A. Harrison, Phys. Rev. 147, 467 (1966).

[7]G. Dresselhaus, M. S. Dresselhaus, and D. Beaglehole, in Proceedings of the Third Materials Research Symposium, Natl. Bur. Std., Gaithersburg (unpublished).

[8]A. I. Golovashkin, A. I. Kopeliovich, and G. P. Motulevich, Zh. Eksperim. i Teor. Fiz. 53, 2053 (1967) [Soviet Phys. JETP 26, 1161 (1968)].

[9]The signs of $c_{\vec{k}}$ and $c_{\vec{k}-\vec{K}}$ depend, as is well known, on the sign of $U_{\vec{K}}$, and hence of γ. Expressions similar to those appearing in Eqs. (1)–(5) have also been used by S. Berko and J. S. Plaskett, Phys. Rev. 112, 1877 (1958), in their analysis of band-edge effects in positron annihilation in metals.

[10]These figures are taken from R. Lück, Aluminium 12, 733 (1969).

[11]See Eq. (14).

[12]P. N. Butcher, Proc. Phys. Soc. (London) 64, 765 (1951). In applying Butcher's result, it has been pointed out by J. Appelbaum [Phys. Rev. 144, 435 (1966)] and A. O. E. Animalu [*ibid.* 163, 557 (1967)] that momentum matrix elements must be evaluated with the true-wave-functions which differ from the pseudo-wave-functions (4) by core orthogonalization terms. For metals with tightly bound cores (as in Al) these corrections are generally small.

[13]On the question of units it is helpful to extract the quantity $\sigma_a = (e^2/\hbar a_0)\,(1/24\pi)$ which has the convenient value 5.48×10^{-14} sec^{-1}.

[14]G. P. Motulevich, Usp. Fiz. Nauk 97, 211 (1969) [Soviet Phys. Usp. 12, 80 (1969)].

[15]The argument is similar to Butcher's. Let the operations of the point group of the crystal be R; the elemental symmetry segment of the zone is that volume which generates the zone upon the accumulated operations R. Now

$$|\langle\psi_{n'R\vec{k}}|\vec{A}\cdot\vec{\nabla}|\psi_{n\vec{R}\vec{k}}\rangle|^2 = |\langle\psi_{n'\vec{k}}|\vec{A}\cdot R\vec{\nabla}|\psi_{n\vec{k}}\rangle|^2$$

and

$$\epsilon_{nR\vec{k}} = \epsilon_{n\vec{k}} .$$

Hence if we restrict (8) to the fraction of $d\vec{k}$ lying within the elemental zone, the contribution from the entire zone can be obtained by summing over R. But this is precisely the same as summing over bounding Bragg planes.

[16]Equation (14) has previously been used by Ehrenreich *et al.* (Ref. 4) and Dresselhaus *et al.* (Ref. 7) in their analysis of the optical properties of Al. It follows straightforwardly from the assumption of the existence of a time of relaxation and the application of Kubo formula for $\sigma(\omega)$. For details, see H. Ehrenreich, in *The Optical Properties of Solids*, edited by J. Tauc (Academic, New York, 1966). The principal result was originally derived by H. Ehrenreich and M. H. Cohen, Phys. Rev. 115, 786 (1959).

[17]Note that Golovashkin *et al.* (Ref. 8) replace the δ function in (7) by a Lorentzian, a procedure which eliminates the induced emission term in (14).

[18]The solution is given in detail in the analysis of the interband absorption in monovalent metals [N. W. Ashcroft and Kurt Sturm (unpublished)].

[19]T. Holstein, Phys. Rev. 88, 1427 (1952); R. B. Dingle, Physica 19, 729 (1953).

[20]T. Holstein, Phys. Rev. 96, 535 (1954); R. N. Gurzhi, Zh. Eksperim. i Teor. Fiz. 33, 660 (1957) [Soviet Phys.

JETP 6, 506 (1958)].

[21]The lack of this structure has been pointed out by A. J. Hughes, D. Jones, and A. H. Lettington, J. Phys. C 2, 102 (1969).

[22]M. A. Biondi and A. I. Gurobadia, Phys. Rev. 166, 667 (1968); L. W. Bos and D. W. Lynch, Phys. Rev. Letters 25, 156 (1970).

[23]The plasma frequency in Al is so high that scattering effects from phonons impurities and surface scattering is unimportant and lifetime effects from electron-electron interactions are beyond the scope of the present investigation.

[24]The optical mass m_{opt} introduced here will be discussed in Sec. V.

[25]C. J. Powell and J. B. Swan, Phys. Rev. 115, 869 (1959).

[26]This point has already been emphasized by J. C. Phillips, Solid State Phys. 18, 55 (1966), in particular, p. 72.

[27]Although it is not *a priori* obvious that the interband relaxation time τ is the same as the intraband equivalent τ_0, it is nonetheless difficult to see how they can differ substantially.

[28]This rule has been established by P. C. Martin, Phys. Rev. 161, 143 (1967), but only insofar as the system (here nearly free-electron-like metals) can be regarded as translationally invariant.

[29]D. Brust, Solid State Commun. 8, 413 (1970).

[30]It follows that knowing V_{200} alone (as given for example by the position of the principal absorption peak), one can determine a bound on V_{111} by using the measured optical mass. (Strictly speaking this will be a bound on the component of the optical pseudopotential.) If this is done in Al the value of V_{111} so obtained is within a few percent of the Fermi-surface predicted value. In other metals this method may give a useful preliminary estimate of (optical) band gaps as well as imposing an overall limitation on their absolute values.

[31]See also the discussion in F. Wooten, E. Pajanne, and B. Bergersen, Phys. Status Solidi 37, 367 (1970).

PHYSICAL REVIEW B VOLUME 3, NUMBER 6 15 MARCH 1971

Correlation Energy of the Electron Gas at Metallic Densities*

John Lam†
Division of Chemistry, National Research Council of Canada, Ottawa 2, Canada
(Received 24 September 1970)

The electron gas at metallic densities is studied by means of a quadratic boson Hamiltonian which includes the direct and exchange processes among the electrons but neglects the scattering of electron-hole pairs. This Hamiltonian is further separated into two independent parts which describe the singlet and triplet states of the electron-hole pairs. These parts are diagonalized in an approximation in which the exchange interaction is treated on the average. A dielectric function for all momentum transfers is thereby obtained. The correlation energy is the sum of the ground-state energies of the singlet and triplet Hamiltonians. Its value, calculated for the metallic density range ($r_s = 1-6$), is found to be about two-thirds of that in the random-phase approximation. It is consequently numerically smaller than most other estimates. The triplet contribution is very considerable. The triplet ground state is predicted to be unstable for $r_s > 9.4$.

I. INTRODUCTION

The correlation energy of an electron gas was defined by Wigner[1] to be the difference between the true ground-state energy and that calculated in the Hartree-Fock approximation. It is a function of the specific interparticle separation r_s, the Bohr radius a_0 being taken as unity. In the high-density ($r_s \ll 1$) and low-density ($r_s \gg 1$) limits, its value has been calculated very accurately by Gell-Mann and Brueckner[2] and Coldwell-Horsfall and Maradudin,[3] respectively. If we regard the electron gas as a model of real metals, we must consider its behavior in the intermediate-density region $1 < r_s < 6$. A number of estimates of the correlation energy at metallic densities have been made by means of interpolation methods. Wigner[4] and Carr and Maradudin[5] have interpolated between the high- and low-density limits. Another method is to interpolate between the contributions from processes of high- and low-momentum transfers, as was done by Hubbard[6] and Nozières and Pines.[7] There is also a variational calculation by Gaskell.[8] These investigations and many others have indicated that the properties of an electron gas even at metallic densities are very similar to those at high density.

It has been shown by Sawada[9] that the high-density results of Gell-Mann and Brueckner can be obtained from a Hamiltonian quadratic in quasiboson operators. These operators describe the creation and annihilation of electron-hole pairs and approximately obey Bose commutation rules at high density. The Sawada Hamiltonian takes into account the direct interaction between electrons in the singlet state, and is equivalent to the random-